Chinese Journal of
POLYMER SCIENCE

ARTICLE

https://doi.org/10.1007/s10118-019-2326-9
Chinese J. Polym. Sci. **2020**, *38*, 187–194

Selective Carbon Dioxide Capture in Antifouling Indole-based Microporous Organic Polymers

Meng-Qi Du[a†], Yu-Zheng Peng[a†], Yuan-Chi Ma[b†], Li Yang[a,b*], Yuan-Lin Zhou[a*], Fan-Kun Zeng[a*], Xiang-Ke Wang[a], Man-Ling Song[a], and Guan-Jun Chang[a,b*]

[a] *State Key Laboratory of Environment-friendly Energy Materials, School of Material Science and Engineering, School of Life Science and Engineering, Southwest University of Science and Technology, Mianyang 621010, China*
[b] *Department of Chemical and Biomolecular Engineering, University of Pennsylvania, Philadelphia, Pennsylvania 19104, United States*

Electronic Supplementary Information

Abstract Intermolecular synergistic adsorption of indole and carbonyl groups induced by intermolecular hydrogen bonding makes microporous organic polymer (PTICBL) exhibit high CO_2 uptake capacity (5.3 mmol·g^{-1} at 273 K) and selectivities (CO_2/CH_4 = 53, CO_2/N_2 = 107 at 273 K). In addition, we find that indole units in the PTICBL networks inhibit the attachment of bacteria (*E. coil* and *S. aureus*) on the surface of PTICBL and extend its service life in CO_2 capture.

Keywords CO_2 capture; Synergistic adsorption; Antifouling; Indole; Microporous organic polymer

Citation: Du, M. Q.; Peng, Y. Z.; Ma, Y. C.; Yang, L.; Zhou, Y. L.; Zeng, F. K.; Wang, X. K.; Song, M. L.; Chang, G. J. Selective carbon dioxide capture in antifouling indole-based microporous organic polymers. *Chinese J. Polym. Sci.* **2020**, *38*, 187–194.

INTRODUCTION

Carbon dioxide emission is mainly from the burning of oil, coal, and energy gas (such as oil gas and natural gas) which constitute the primary source of energy for economic development, industrial production, and even our daily life.[1–5] Before the realization of alternative cleaner energy or energy technology,[6,7] CO_2 emissions in the atmosphere will continue to increase.[8,9] It is thus so significant and obligated for us to study novel adsorbents to reduce their environmental impact. In recent years, indole is considered as a functionality of CO_2 uptake *via* local dipole-π interaction.[10,11] Later, we have confirmed that high and selective CO_2 capture can be carried out *via* intramolecular synergistic effects of bifunctional indole and their adjacent functional groups (such as amide or carbonyl groups).[11,12] Generally, a huge bifunctional unit should be synthesized and introduced into the microporous organic polymers (MOPs) to achieve the intramolecular synergistic effects on CO_2, which will increase the cost of MOPs. In order to reduce the cost and maintain high and selective CO_2 capture of the resulting MOPs, in this work, we synthesized a facial indole-based MOP with carbonyl (C=O) and imino (NH) groups in the polymer network. Hydrogen bonding between the polymer chains can shorten the distance between C=O and NH of indole, leading to intermolecular adsorption. It was expected that the indole and carbonyl bifunctional groups between the polymer chains would exert effective intermolecular synergistic effects that is essential requirements for CO_2 capture.[14–16]

As we know, the surface of materials is susceptible to bacterial attachment and further formation of a biofilm due to the mutual attachment among bacteria cells after a long-term recycle in practice,[17–19] which will block the porous, reduce specific surface area, and decrease the CO_2 uptake capacity. Indole and its derivatives as natural antifouling materials can effectively inhibit bacterial growth and reproduction due to a strong inhibition for DNA replication and protein synthesis of bacteria.[20–23] Bearing this in mind, we expected that the indole-based microporous organic polymer obtained in this work would exhibit encouraging antifouling property and extend its service life working in CO_2 capture.

To demonstrate the concept, a simple functional monomer, 1,3,5-tris(3-indolcarbonyl)benzene (TICB), was successfully synthesized by a traditional Friedel-Crafts acylation reaction using indole and 1,3,5-benzenetricarbonyl trichloride as the monomers.[24] The resulting TICB was polymerized with dimethoxy methane (DMM) *via* Friedel-Crafts reaction catalyzed by $FeCl_3$ (Fig. 1a),[25,26] and then indole-based MOP (PTICBL) can be easily obtained (see the electronic supplementary information, ESI, for details). As-prepared PTICBL was

* Corresponding authors, E-mail: yanglichem628@126.com (L.Y.)
E-mail: zhouyuanlin@swust.edu.cn (Y.L.Z)
E-mail: fkzeng920924@163.com (F.K.Z)
E-mail: gjchang@mail.ustc.edu.cn (G.J.C.)
† These authors contributed equally to this work.
Received May 25, 2019; Accepted July 1, 2019; Published online September 29, 2019

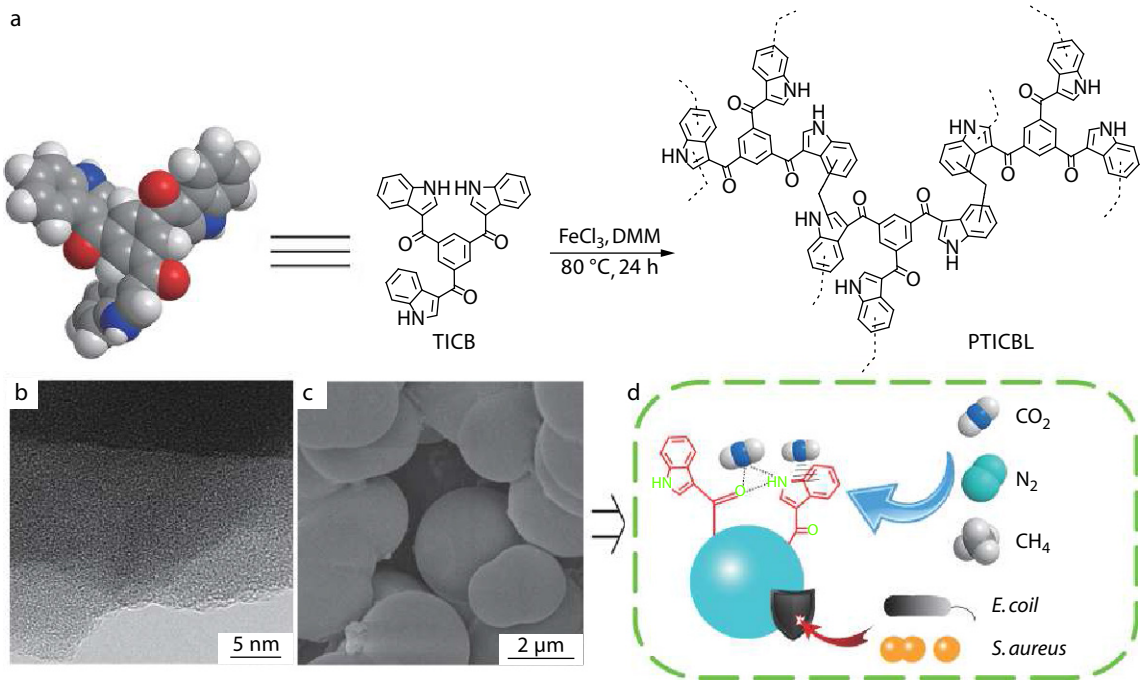

Fig. 1 (a) The structure of monomer (TICB) and the synthetic route to PTICBL; Micro-structures of the PTICBL network: (b) TEM and (c) SEM images; (d) The intermolecular synergistic adsorption mechanism of indole and carbonyl units on CO_2 uptake in antifouling PTICBL network.

characterized by ^{13}C CP/MAS NMR, FTIR, and elemental analysis, and the results agreed with the proposed structures (Fig. 2). In this work, gas adsorption capacities, selectivities, the isosteric heat, and antifouling properties were investigated. As we expected, the indole-based MOP (PTICBL) exhibited high CO_2 uptake capacity with high selectivity owing to the intermolecular synergistic adsorption of indole and carbonyl unit toward CO_2 (Fig. 1d). Additionally, the indole-based PTICBL network showed encouraging antifouling behaviour, such as *Staphylococcus aureus* (*S. aureus*) and *Escherichia coli* (*E. coli*), which lay the foundation for extending its service life in CO_2 capture.

EXPERIMENTAL

Materials, measurements, and synthetic routes of the monomer and MOPs, physical properties of the resulting MOPs, and antifouling capability testing are described in ESI.

RESULTS AND DISCUSSION

In order to confirm the successful formation of microporous polymer, PTICBL was characterized at molecular levels by using FTIR spectrometry and ^{13}C CP/MAS NMR spectrometry. FTIR spectrum of the microporous organic polymer is shown in Fig. 2(a), where the absorption bands at about 2962 and 3415 cm^{-1} correspond to the structure of methylene and NH in the indole groups, respectively. The structural information of the prepared PTICBL was also obtained by ^{13}C CP/MAS NMR spectroscopy (Fig. 2b). There are three broad signals at 186, 150–75, and 38 ppm. The signal at about 186 ppm is ascribed to the carbonyl group carbons (Fig. 2b and Scheme S1 in ESI), and the broad signals at 150–75 ppm are ascribed to the indole group and

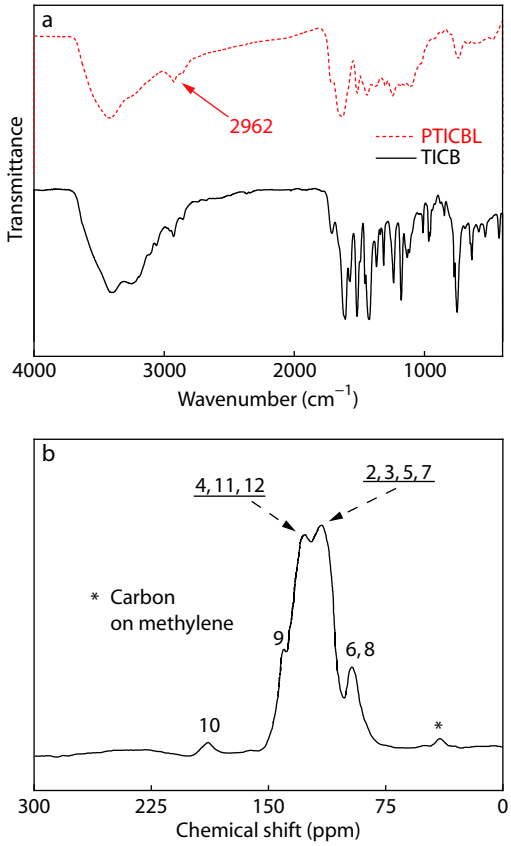

Fig. 2 (a) FTIR spectra of indole-based microporous organic polymer (PTICBL) and 1,3,5-tris-(3-indolcarbonyl)benzene (TICB); (b) ^{13}C CP/MAS NMR spectrum of indole-based microporous organic polymer (PTICBL).

https://doi.org/10.1007/s10118-019-2326-9

benzene carbons (Fig. 2b). The signal at about 38 ppm corresponds to methylene carbons between indole groups, which is perfectly consistent with a previous study about carbazole-based porous organic polymer.[15]

Microstructure is an important factor for MOPs materials, which determines their application in CO_2 uptake. SEM image displays that PTICBL contained aggregated particles around 3 μm in diameter (Fig. 1c), and TEM image (Fig. 1b) shows the microporous structure of PTICBL, which plays an important role in CO_2 adsorption and separation. Microporous structure means high specific surface area and facilitates carbon dioxide loading. The pore size distribution and specific surface area of PTICBL were determined by nitrogen (77 K) adsorption-desorption method and the results are shown in Fig. 3(a). At a low pressure (0–0.01 MPa), the nitrogen adsorption-desorption isotherm rose rapidly at 77 K, which reflected the properties of microporous structure, consistent with the results of the TEM image. The pore size distribution (PSD) of

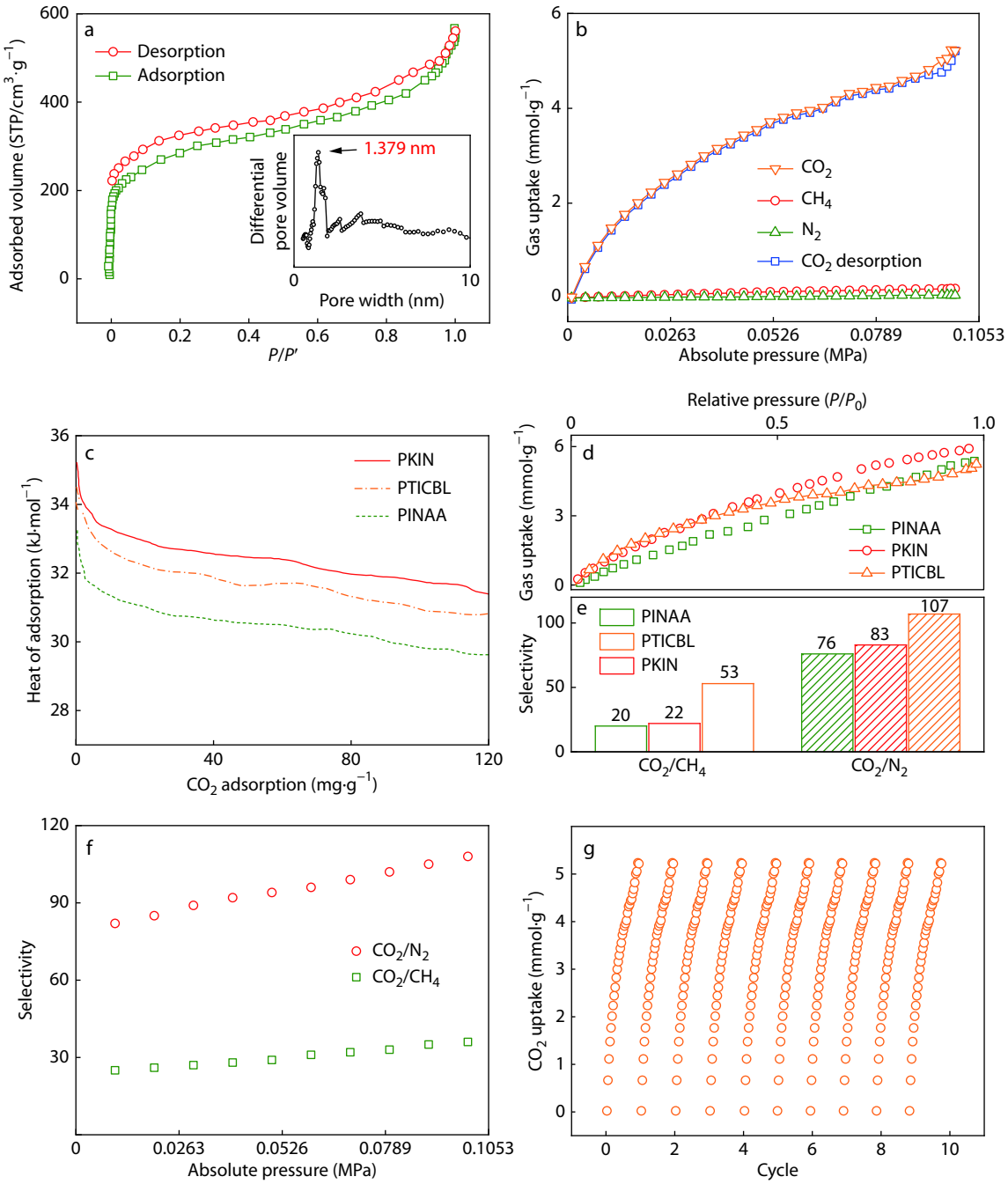

Fig. 3 (a) N_2 adsorption-desorption isotherm curves and the pore size distribution (inset) of PTICBL at 77 K; (b) Adsorption and desorption isotherm curves of PTICBL for different gases at 273 K; (c) Heat of adsorption of PINAA,[13] PKIN,[12] and PTICBL; (d) Isothermal adsorption curve for CO_2 adsorption at 273 K of PINAA, PKIN, and PTICBL; (e) CO_2/N_2 and CO_2/CH_4 adsorption selectivity of PINAA, PKIN, and PTICBL; (f) IAST selectivity (CO_2:N_2 = 15:85, CO_2:CH_4 = 5:95) at 298 K; (g) Cycles of CO_2 adsorption for PTICBL at 273 K.

https://doi.org/10.1007/s10118-019-2326-9

PTICBL was approximated by local density functional theory (NLDFT) using a cylindrical oxide pore surface model.[27] The calculation yielded a sharp peak at 1.379 nm. At relatively high pressure (0.09 MPa), the increasing nitrogen adsorption owing to inter-particulate voids was related to the meso- and macrostructure of the sample. Data calculation showed that the specific surface area of PTICBL by Brunauer-Emmett-Teller (BET) method was up to 1237 $m^2 \cdot g^{-1}$. In addition, PTICBL network showed good thermal property in a nitrogen atmosphere (Fig. S5 in ESI).[12,26,28]

The CO_2 adsorption capacity and selectivities (CO_2/N_2 and CO_2/CH_4) of PTICBL at 273 K were characterized, as shown in Fig. 3(b); the CO_2 adsorption capacity rose with the increasing pressure, whereas the increase of N_2 or CH_4 adsorption capacity was negligible. The CO_2 adsorption capacity of PTICBL at 273 K was as high as 5.3 $mmol \cdot g^{-1}$, while that of CH_4 and N_2 were only 0.21 and 0.06 $mmol \cdot g^{-1}$, respectively (Fig. 3b). According to initial slope fitting at 273 K for PTICBL (Fig. S7 in ESI), the adsorption selectivities (CO_2/N_2 and CO_2/CH_4) were approximately 107 and 53 (Figs. 3d and 3e). Gas uptake isotherms at 291, 298, and 308 K are shown in Fig. S6 (in ESI). Equilibrium CO_2 adsorption capacity is found to decrease with an increase in temperature (Fig. S8 in ESI) due to the exothermic nature of the adsorption process, as expected for physical adsorbents. Compared with our previous indole-based MOPs, PINAA[13] and PKIN,[12] the PTICBL network showed comparable CO_2 uptake capacity and higher selectivity (Figs. 3d and 3e) due to the following two reasons: (1) PTICBL network exhibited multiple mechanisms working for CO_2 adsorption such as local dipole-π interactions, hydrogen bonding, and dipole-quadrupole between sorbated gas molecule and the adsorbent; (2) because of the intermolecular hydrogen bonding, intermolecular synergistic adsorption was formed between indole and carbonyl units from two different polymer chains, which is beneficial to the increase of CO_2 selectivity.[11] In addition, we found the CO_2 adsorption capacity and selectivity of PTICBL polymer were higher than those of a large number of CO_2 capture porous materials (Table S6 in ESI).

In real industrial applications, the flue gas from a power plant is a mixture of CO_2, water vapor, and others. It is known that water vapor tends to prevent CO_2 adsorption.[29] Here, we quantified the CO_2 capture performance under a wet condition (Fig. S9 in ESI). The CO_2 adsorption capacity of PTICBL decreased from 5.3 $mmol \cdot g^{-1}$ to 3.7 $mmol \cdot g^{-1}$ (0.1 MPa, 273 K) in the presence of water vapor [relative humidity (RH) = 3%]. The presence of water vapor did not influence CH_4 and N_2 capture in PTICBL. These results indicate that water may occupy some strong adsorption sites, while the capture of CH_4 and N_2 is nonspecific. Overall, although the selectivity (CO_2/N_2 = 65; CO_2/CH_4 = 43) was decreased under humid conditions, PTICBL, to the best of our knowledge, still has the highest CO_2 selectivity over other CO_2 capture materials in similar conditions.[30]

Isothermal adsorption models, *e.g.* Langmuir, Freundlich, and Temkin, are widely used to analyse adsorption phenomena. The results of nonlinear fitting of isothermal adsorption curves are shown in Figs. S10–S12 and Tables S1–S3 (in ESI). The Langmuir isotherm and the Freundlich isotherm both fit quite well with experimental data (correlation coefficient $R^2 > 0.95$). Therefore, a better criterion to evaluate experimental isotherm data is a parameter called normalized percent deviation (*P*), and the details can be found in ESI. The *P*-values calculated from the Langmuir model were lower than that from the Freundlich model and below the value of 5, which can give conclusion that the CO_2 adsorption behaviour of PTICBL could be better described by the Langmuir isotherm. The selectivity level at 298 K was calculated by the theory of ideal adsorption solution (IAST). The theory predicts the adsorption selectivity of mixed gases according to the pure-component gas isotherms. The results are displayed in Fig. 3(f).

Furthermore, the adsorption behaviour of PTICBL was conveniently predicted by the adsorption kinetic models, and the results can be seen in Fig. S13 and Table S4 (in ESI). Pseudo-first model (correlation coefficient $R^2 = 0.99$) better described the adsorption behaviour of PTICBL than pseudo-second model did, indicating the reversible interaction between adsorbent and adsorbate which was suitable to predict the CO_2 adsorption behaviour on physical adsorbent.[31] Furthermore, reversible adsorption/desorption behaviour could be well achieved by vacuuming the system even though small hysteresis existed in the desorption branch (Fig. 3b); this is beneficial to the recycling of PTICBL. The reversibility of CO_2 adsorption on PTICBL at 273 K was further characterized over 10 cycles. As shown in Fig. 3(g), the CO_2 adsorption capacities were nearly identical for 10 cycles, which suggests that PTICBL possesses a great recyclability.

The isosteric heat of adsorption (Q_{st}) of the binding affinity of CO_2 to the resulting material was calculated by the method of virial analysis.[32] As shown in Fig. 3(c) and Fig. S14 (in ESI), PTICBL had a Q_{st} value of 34.5 $kJ \cdot mol^{-1}$ at low adsorption values. The high Q_{st} value indicates that the combination of indole and carbonyl unit can be considered as an effective synergetic unit for fast CO_2 capture.

To illustrate the capture mechanism, we used DFT[33] to investigate the mechanism of intermolecular synergistic adsorption induced by intermolecular hydrogen bonding during CO_2 uptake. The calculation is detailed in ESI. Fig. 4 shows a series of snapshots of carbon dioxide captured by model compounds, in which indole and carbonyl units worked synergistically to capture several carbon dioxide molecules. Fig. 4 shows a minimized geometry of the model compounds. As presented in Fig. 4(a), the hydrogen bonding between C=O and NH groups established and formed intermolecular adsorption unit.[33–36] The CO_2 uptake process can be described as follows. (1) The first CO_2 molecule could be captured on the indole ring due to its relatively large binding area (Fig. 4b), and the calculated binding energy of CO_2 with indole was 18.2 $kJ \cdot mol^{-1}$ (Fig. S15 in ESI). For the CO_2-indole complex, the minimum energy structure was obtained when CO_2 lay on the indole ring at a distance of 3.16 Å to form the local dipole-π conformation (Fig. 4b).[13] (2) With the help of an adjacent indole, conformation of the CO_2-carbonyl-imine group complex was formed while maintaining the high selectivities of CO_2 over other gas molecules (Figs. 4c and 4d),[11,13] and the calculated binding energy of CO_2 on carbonyl-imine unit was 19.5 $kJ \cdot mol^{-1}$ (Fig. S15 in ESI). (3) The second CO_2 molecule could be adsorbed on the indole group *via* the local dipole-π inter-

https://doi.org/10.1007/s10118-019-2326-9

actions (Figs. 4e and 4f). According to the calculation result, we can find that the synergistic effect of multiple interactions of indole and carbonyl units with CO_2 was successfully generated which also has the same phenomenon in the polymer (Fig. S17 in ESI), and this is why PTICBL showed a higher selectivity compared with our published works.[12,13,37] Referring to the $-\Delta E_e$ value of model compound-CO_2 (18.2 and 19.5 kJ·mol^{-1}), lower $-\Delta E_e$ of model compound-CH_4 and N_2 implies strong interaction between CO_2 and adsorbate (Fig. S20 in ESI).

According to the previous work,[12] there is no intermolecular hydrogen bonding on carbonyl group of PKIN with full CO_2 (Table S5 in ESI). Hence, compared with PKIN, the red shift of the band of carbonyl group in PTICBL after absorbing CO_2 in-

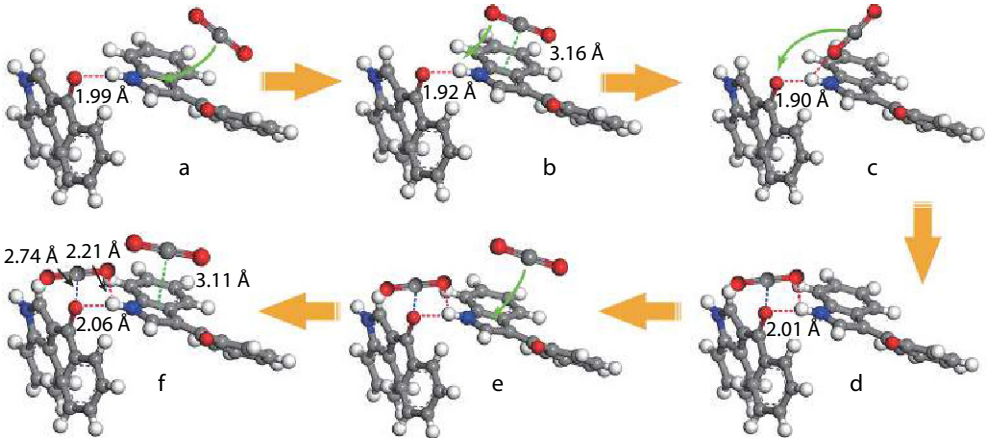

Fig. 4 DFT results for tracking the entire carbon dioxide capture process. (a, b) The face of an indole with electron-rich π heteroaromatic ring can adsorb a CO_2 molecule by the local dipole-π interaction. (c, d) An adjacent carbonyl and NH group can capture a desorbed CO_2 molecule. (e, f) Another CO_2 molecule is closing to the face of indole ring by the local dipole-π interaction. The grey, blue, white, and red spheres represent carbon, nitrogen, hydrogen, and oxygen atoms; the green, blue, and red dotted line represent the local dipole-π, dipole-quadrupole interaction, and hydrogen bonding, respectively.

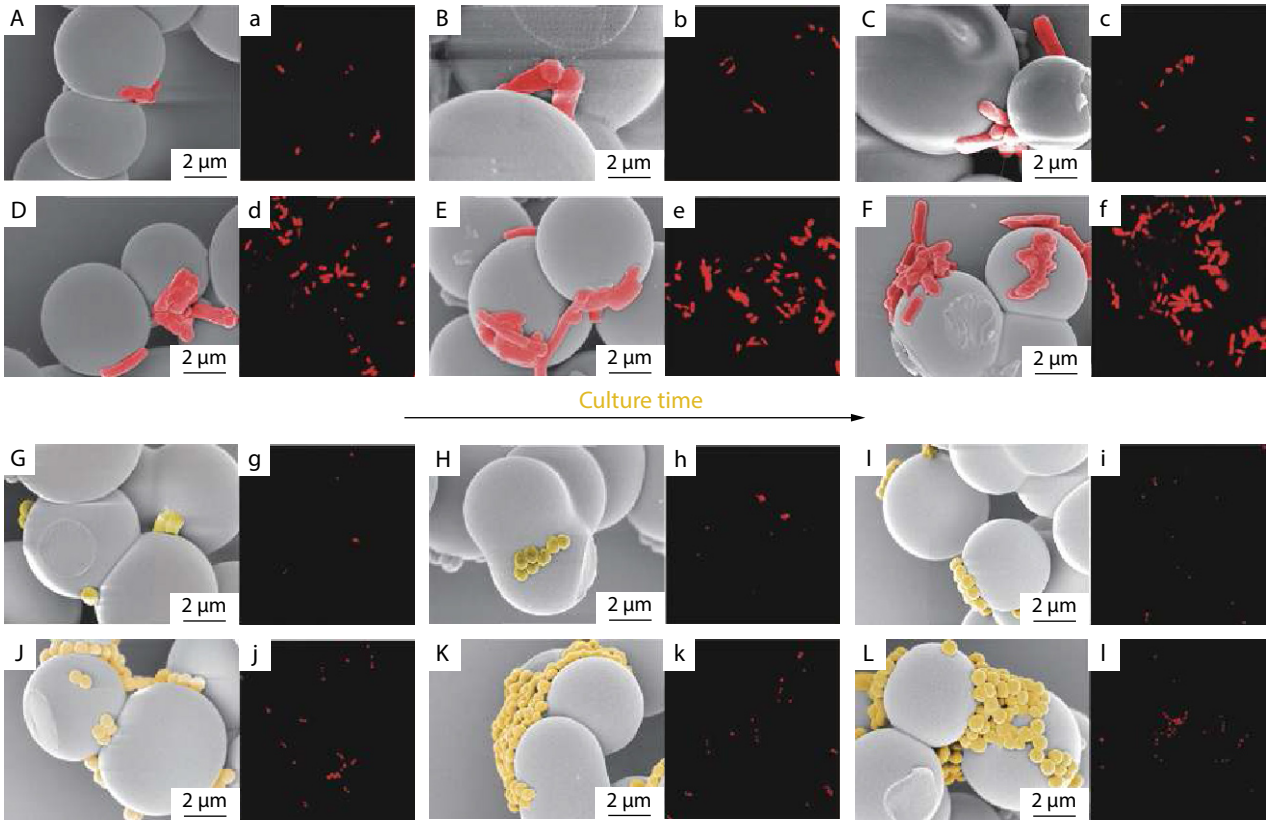

Fig. 5 The microscopic images at the same magnification of bacteria attachment after 2, 10, and 24 h of culture time: (A–L) SEM images, and (a–l) LSCM images. (A–C, a–c) PTICBL for *E. coli*; (D–F, d–f) RF aerogel for *E. coli*; (G–I, g–i) PTICBL for *S. aureus*; (J–L, j–l) RF aerogel for *S. aureus*.

https://doi.org/10.1007/s10118-019-2326-9

dicated intermolecular hydrogen bonding between carbonyl and imine group (Fig. S3 in ESI). As for PINAA network, intermolecular hydrogen bonding was not formed due to strong *π*-*π* stacking interaction (Fig. S16 in ESI). Additionally, the existence of methyl groups in PTICBL provided the possibility of intermolecular synergistic adsorption induced by intermolecular hydrogen bonding (Figs. S18 and S19 in ESI).

Gram-negative and gram-positive representative bacteria, *Escherichia coli* (*E. coli*) and *Staphylococcus aureus* (*S. aureus*), have been widely used for discussing antifouling capability of materials.[38–42] In this work, the antifouling capability of the resulting PTICBL network was characterized with *E. coli* and *S. aureus*. In order to further understand the antifouling capability of PTICBL network, the traditional Resorcin-Formaldehyde (RF) network with similar microstructure was also constructed (see ESI). PTICBL and RF were separately immersed in *E. coli* and *S. aureus* suspension, and the inoculated surfaces were then incubated in fresh modified Luria Broth (LB) at 37 °C for 2, 10, and 24 h. After centrifugation and stratification, the samples were soaked in 2.5% glutaraldehyde solution to fix bacteria on their surface, rinsed with phosphate buffered saline (PBS) three times to get rid of bacteria not adhered to the polymer surface and guarantee the shape and activity of bacteria, and washed with ethanol to gradient dehydration. After vacuum-dried, the attachment of bacteria on the surface of the samples was observed by scanning electron microscopy (SEM). As shown in Figs. 5(A)–5(L), the surface of indole-based microporous organic polymer PTICBL was attached by less *E. coli* and *S. aureus* than that of the RF aerogel at same culturing time, indicating that the resulting indole-based PTICBL exhibited compelling antifouling capability.

The area fraction covered by *E. coli* and *S. aureus* was calculated by images of laser scanning confocal microscopy (LSCM) in order to further discuss the attachment of bacteria on the surface of PTICBL and RF. The samples were stained with SYTO 9 about 20 min for confocal imaging, and the results are displayed in Figs. 5(a)–5(i) and 6. Indole-based microporous organic polymer (PTICBL) showed a lower coverage rate, 2.061% of *E. coli* and 0.539% of *S. aureus*, than that of traditional RF, about 13.223% and 1.593%, as the existence of indole group effectively inhibited bacterial growth and reproduction.[19–22] Compared with other porous materials, PTICBL exhibits excellent adhesion resistance to *E. coli* and *S. aureus* (Table S7 in ESI). In addition, the coverage rate of *E. coli* was higher than that of *S. aureus* due to different susceptibility of these bacteria to indole-based PTICBL, which potentially depends upon their cell structure such as the absence of *S. aureus* outer membrane.[43] Importantly, the CO_2 adsorption capacity of PTICBL after 24 h of culture time was also characterized and the results are shown in Fig. 6(c). The CO_2 adsorption capacity of PTICBL after bacteria attachment at 273 K was decreased (4.1 mmol·g^{-1} of *S. aureus*, 3.7 mmol·g^{-1} of *E. coli*) due to the reduction of specific surface area. The adsorption capacity of PTICBL after *S. aureus* attachment was higher than that of PTICBL after *E. coli* attachment, which is owing to the more area coverage of *E. coli* colonization on the surface of PTICBL. However, the CO_2 adsorption capacity of PTICBL after bacteria attachment was comparable with other MOPs (Table S6 in ESI).

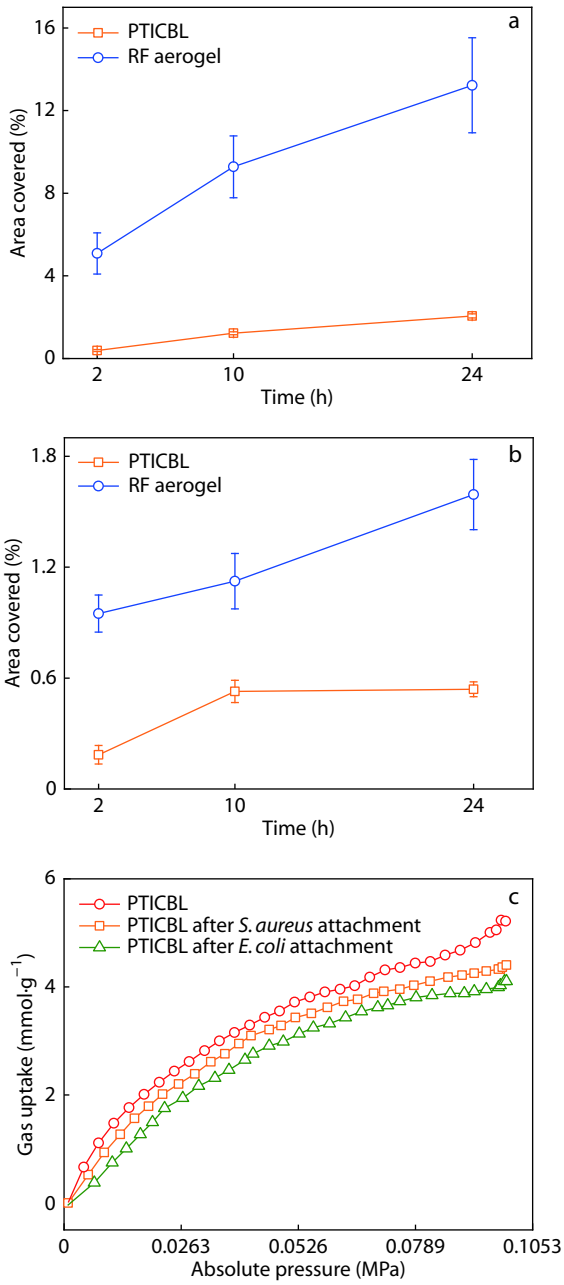

Fig. 6 Area coverage of bacteria colonization calculated by confocal images after inoculation of 2, 10, and 24 h on PTICBL and the traditional RF aerogel: (a) *E. coli* and (b) *S. aureus*; (c) CO_2 adsorption capacity of PTICBL after 24 h bacterial culturing.

CONCLUSIONS

In summary, the indole-based microporous organic polymer (PTICBL) was prepared by one-step Friedel-Crafts reaction and applied as CO_2 adsorption material. Taking advantage of the intermolecular synergistic adsorption of indole and carbonyl groups induced by intermolecular hydrogen bonding, the PTICBL network exhibited encouraging CO_2 adsorption capacity and selectivity (5.3 mmol·g^{-1}, CO_2/N_2 = 107, CO_2/CH_4 = 53 at 273 K). The key innovation of this work includes two aspects: first, the facial construction technology can reduce the produc-

https://doi.org/10.1007/s10118-019-2326-9

tion costs and maintain high CO_2 capture properties for the resulting PTICBL; second, PTICBL can efficiently inhibit the attachment of bacteria on the surface to extend its service life in CO_2 capture. Taken together, the structure design of PTICBL is expected to be a new rationale for fabrication of high CO_2 capture materials with long service life.

Electronic Supplementary Information

Electronic supplementary information (ESI) is available free of charge in the online version of this article at http://dx.doi.org/10.1007/s10118-019-2326-9.

ACKNOWLEDGMENTS

This work was financially supported by the National Natural Science Foundation of China (Nos. 11447215, 21202134, and 21504073), the Scientific Research Fund of Sichuan Provincial Education Department (Nos. 18ZA0495 and 16ZA0136), the Sichuan Youth Science & Technology Foundation (Nos. 2016JQ0055), the Longshan academic talent research supporting program of SWUST (Nos. 18LZX446 and 18LZX308), the Student's Platform for Innovation and Entrepreneurship Training Program (No. 201710619013). Guanjun Chang and Li Yang are grateful for financial support from the China Scholarship Council.

REFERENCES

1 Tian, K.; Zhu, T. T.; Lan, P.; Wu, Z. C.; Hu, W.; Xie, F. F.; Li, L. Massive preparation of coumarone-indene resin-based hyper-crosslinked polymers for gas adsorption. *Chinese J. Polym. Sci.* **2018**, *36*, 1168–1174.
2 Shakun, J. D.; Clark, P. U.; He, F.; Marcott, S. A.; Mix, A. C.; Liu, Z.; Otto-Bliesner, B.; Schmittner, A.; Bard, E. Global warming preceded by increasing carbon dioxide concentrations during the last deglaciation. *Nature* **2012**, *484*, 49–54.
3 Gan, C. J.; Xu, X. C.; Jiang, X. W.; Gan, F.; Dong, J.; Zhao, X.; Zhang, Q. H. Fabrication of 6FDA-HFBAPP polyimide asymmetric hollow fiber membranes and their CO_2/CH_4 separation properties. *Chinese J. Polym. Sci.* **2019**, *37*, 815–826.
4 Zhou, Z.; Anderson, C. M.; Butler, S. K.; Thompson, S. K.; Whitty, K. J.; Shen, T.; Stowers, K. J. Stability and efficiency of CO_2 capture using linear amine polymer modified carbon nanotubes. *J. Mater. Chem. A* **2017**, *5*, 10486–10494.
5 DeConto, R. M.; Pollard, D. Contribution of Antarctica to past and future sea-level rise. *Nature* **2016**, *531*, 591–597.
6 Wei, W.; Chang, G.; Xu, Y.; Yang, L. An indole-based conjugated microporous polymer: A new and stable lithium storage anode with high capacity and long life induced by cation-π interactions and a N-rich aromatic structure. *J. Mater. Chem. A* **2018**, *6*, 18794–18798.
7 Wang, K.; Yang, L.; Wei, W.; Zhang, L.; Chang, G. Phosphoric acid-doped poly(ether sulfone benzotriazole) for high-temperature proton exchange membrane fuel cell applications. *J. Membr. Sci.* **2018**, *549*, 23–27.
8 Xiang, S.; He, Y.; Zhang, Z.; Wu, H.; Zhou, W.; Krishna, R.; Chen, B. Microporous metal-organic framework with potential for carbon dioxide capture at ambient conditions. *Nat. Commun.* **2012**, *3*, 954–962.
9 Wang, R.; Moreno-Cruz, J.; Caldeira, K. Will the use of a carbon tax for revenue generation produce an incentive to continue carbon emissions? *Environ. Res. Lett.* **2017**, *12*, 6–14.
10 Chang, G.; Shang, Z.; Yu, T.; Yang, L. Rational design of a novel indole-based microporous organic polymer: enhanced carbon dioxide uptake *via* local dipole-π interactions. *J. Mater. Chem. A* **2016**, *4*, 2517–2523.
11 Lee, H. M.; Youn, I. S.; Saleh, M.; Lee, J. W.; Kim, K. S. Interactions of CO_2 with various functional molecules. *Phys. Chem. Chem. Phys.* **2015**, *17*, 10925–10933.
12 Chang, G.; Xu, Y.; Zhang, L.; Yang, L. Enhanced carbon dioxide capture in an indole-based microporous organic polymer *via* synergistic effects of indoles and their adjacent carbonyl groups. *Polym. Chem.* **2018**, *9*, 4455–4459.
13 Yang, L.; Chang, G.; Wang, D. High and selective carbon dioxide capture in nitrogen-containing aerogels *via* synergistic effects of electrostatic in-plane and dispersive π-π-stacking interactions. *ACS Appl. Mater. Interfaces* **2017**, *9*, 15213–15218.
14 Rabbani, M. G.; Reich, T. E.; Kassab, R. M.; Jackson, K. T.; El-Kaderi, H. M. High CO_2 uptake and selectivity by triptycene-derived benzimidazole-linked polymers. *Chem. Commun.* **2012**, *48*, 1141–1143.
15 Saleh, M.; Lee, H. M.; Kemp, K. C.; Kim, K. S. Highly stable CO_2/N_2 and CO_2/CH_4 selectivity in hyper-cross-linked heterocyclic porous polymers. *ACS Appl. Mater. Interfaces* **2014**, *6*, 7325–7333.
16 Islamoglu, T.; Behera, S.; Kahveci, Z.; Tessema, T. D.; Jena, P.; El-Kaderi, H. M. Enhanced carbon dioxide capture from landfill gas using bifunctionalized benzimidazole-linked polymers. *ACS Appl. Mater. Interfaces* **2016**, *8*, 14648–14655.
17 Bazaka, K.; Jacob, M. V.; Crawford, R. J.; Ivanova, E. P. Efficient surface modification of biomaterial to prevent biofilm formation and the attachment of microorganisms. *Appl. Microbiol. Biot.* **2012**, *95*, 299–311.
18 Arciola, C. R.; Campoccia, D.; Speziale, P.; Montanaro, L.; Costerton, J. W. Biofilm formation in *Staphylococcus* implant infections. A review of molecular mechanisms and implications for biofilm-resistant materials. *Biomaterials* **2012**, *33*, 5967–5982.
19 Hasan, J.; Crawford, R. J.; Ivanova, E. P. Antibacterial surfaces: the quest for a new generation of biomaterials. *Trends Biotechnol.* **2013**, *31*, 295–304.
20 Chen, M.; Wang, K.; Wang, C. Antifouling indole alkaloids of a marine-derived fungus *Eurotium* sp. *Chem. Nat. Compd.* **2018**, *54*, 207–209.
21 Fang, K.; Li, X.; Yu, L. Synthesis, antibacterial activity, and application in the antifouling marine coatings of novel acylamino compounds containing gramine groups. *Prog. Org. Coat.* **2018**, *118*, 141–147.
22 Feng, D.; He, J.; Chen, S.; Su, P.; Ke, C.; Wang, W. The plant alkaloid camptothecin as a novel antifouling compound for marine paints: laboratory bioassays and field trials. *Mar. Biotechnol.* **2018**, *20*, 623–638.
23 Qi, S.; Ma, X. Antifouling compounds from marine invertebrates. *Mar. Drugs* **2017**, *15*, 263–282.
24 Guchhait, S. K.; Kashyap, M.; Kamble, H. $ZrCl_4$-mediated regio- and chemoselective Friedel-Crafts acylation of indole. *J. Org. Chem.* **2011**, *76*, 4753–4758.
25 Li, B.; Gong, R.; Wang, W.; Huang, X.; Zhang, W.; Li, H.; Hu, C.; Tan, B. A new strategy to microporous polymers: knitting rigid aromatic building blocks by external cross-linker. *Macromolecules* **2011**, *44*, 2410–2414.
26 Saleh, M.; Baek, S. B.; Lee, H. M.; Kim, K. S. Triazine-based microporous polymers for selective adsorption of CO_2. *J. Phys. Chem. C* **2015**, *119*, 5395–5402.
27 Vishnyakov, A.; Ravikovitch, P. I.; Neimark, A. V. Molecular level models for CO_2 sorption in nanopores. *Langmuir* **1999**, *15*, 8736–8742.

28 Yang, P.; Yang, L.; Yang, J.; Luo, X.; Chang, G. Synthesis of a metal-coordinated *N*-substituted polybenzimidazole pyridine sulfone and method for the nondestructive analysis of thermal stability. *High Perform. Polym.* **2019**, *31*, 238–246.
29 Kizzie, A. C.; Wong-Foy, A. G.; Matzger, A. J. Effect of humidity on the performance of microporous coordination polymers as adsorbents for CO_2 capture. *Langmuir* **2011**, *27*, 6368–6373.
30 Liu, J.; Tian, J.; Thallapally, P. K.; McGrail, B. P. Selective CO_2 capture from flue gas using metal-organic frameworks—a fixed bed study. *J. Phys. Chem. C* **2012**, *116*, 9575–9581.
31 Song, G.; Zhu, X.; Chen, R.; Liao, Q.; Ding, Y. D.; Chen, L. An investigation of CO_2 adsorption kinetics on porous magnesium oxide. *Chem. Eng. J.* **2016**, *283*, 175–183.
32 Lehn, J. M. Supramolecular polymer chemistry—scope and perspectives. *Polym. Int.* **2002**, *51*, 825–839.
33 Lehn, J. M. Dynamers: dynamic molecular and supramolecular polymers. *Prog. Polym. Sci.* **2005**, *30*, 814–831.
34 Fox, J. D.; Rowan, S. J. Supramolecular polymerizations and main-chain supramolecular polymers. *Macromolecules* **2009**, *42*, 6823–6835.
35 Brunsveld, L.; Folmer, B. J. B.; Meijer, E. W.; Sijbesma, R. P. Supramolecular polymers. *Chem. Rev.* **2001**, *101*, 4071–4098.
36 Balzer, C.; Cimino, R. T.; Gor, G. Y.; Neimark, A. V.; Reichenauer, G. Deformation of microporous carbons during N_2, Ar, and CO_2 adsorption: Insight from the density functional theory. *Langmuir* **2016**, *32*, 8265–8274.
37 Yang, P.; Yang, L.; Wang, Y.; Song, L.; Yang, J.; Chang, G. An indole-based aerogel for enhanced removal of heavy metals from water *via* the synergistic effects of complexation and cation-π interactions. *J. Mater. Chem. A* **2019**, *7*, 531–539.
38 Wu, Q.; Chen, G.; Sun, W.; Xu, Z.; Kong, Y.; Zheng, X.; Xu, S. Bio-inspired GO-Ag/PVDF/F127 membrane with improved anti-fouling for natural organic matter (NOM) resistance. *Chem. Eng. J.* **2017**, *313*, 450–460.
39 Xie, Y.; Tang, C.; Wang, Z.; Xu, Y.; Zhao, W.; Sun, S.; Zhao, C. Co-deposition towards mussel-inspired antifouling and antibacterial membranes by using zwitterionic polymers and silver nanoparticles. *J. Mater. Chem. B* **2017**, *5*, 7186–7193.
40 Zhang, X.; Shu, Y.; Su, S.; Zhu, J. One-step coagulation to construct durable anti-fouling and antibacterial cellulose film exploiting Ag@AgCl nanoparticle-triggered photo-catalytic degradation. *Carbohyd. Polym.* **2018**, *181*, 499–505.
41 Zhang, X.; Zhang, J.; Yu, J.; Zhang, Y.; Cui, Z.; Sun, Y.; Hou, B. Fabrication of $InVO_4/AgVO_3$ heterojunctions with enhanced photocatalytic antifouling efficiency under visible-light. *Appl. Catal. B-Environ.* **2018**, *220*, 57–66.
42 Samantaray, P. K.; Madras, G.; Bose, S. PVDF/PBSA membranes with strongly coupled phosphonium derivatives and graphene oxide on the surface towards antibacterial and antifouling activities. *J. Membr. Sci.* **2018**, *548*, 203–214.
43 Bindhu, M. R.; Umadevi, M. Antibacterial and catalytic activities of green synthesized silver nanoparticles. *Spectrochimica Acta Part A* **2015**, *135*, 373–378.

https://doi.org/10.1007/s10118-019-2326-9